AGU ADVANCING EARTH AND SPACE SCIENCE

JGR Solid Earth

RESEARCH ARTICLE
10.1029/2020JB020309

Electrical Conductivity of Ti-Bearing Hydrous Olivine Aggregates at High Temperature and High Pressure

Lidong Dai[1,2] and **Shun-ichiro Karato**[2]

[1]Key Laboratory of High-Temperature and High-Pressure Study of the Earth's Interior, Institute of Geochemistry, Chinese Academy of Sciences, Guiyang, China, [2]Department of Earth and Planetary Sciences, Yale University, New Haven CT, USA

Key Points:

- Ti has a strong effect on electrical conductivity of sample; however, its influence is completely different in H-rich and H-poor regimes
- Defect models to explain these observations are proposed by interaction of Ti-related and H-related defects and hopping of small polaron
- It is suggested that the applications of results from Ti-rich olivine samples to the Ti-poor real Earth need to be made with great care

Correspondence to:
L. Dai,
dailidong@vip.gyig.ac.cn

Citation:
Dai, L., & Karato, S.-i. (2020). Electrical conductivity of Ti-bearing hydrous olivine aggregates at high temperature and high pressure. *Journal of Geophysical Research: Solid Earth*, *125*, e2020JB020309. https://doi.org/10.1029/2020JB020309

Received 1 JUN 2020
Accepted 23 SEP 2020
Accepted article online 26 SEP 2020

Abstract We investigated the electrical conductivity of Ti-H-doped synthetic olivine aggregates at 4 GPa, 873–1273 K, and controlled oxygen fugacities. Under a given pressure and temperature, electrical conductivity depends on both hydrogen and Ti content, but these samples show different conductivity behavior from that observed in Ti-poor sample such as San Carlos olivine. We found that when Ti content is comparable to or larger than hydrogen content, Ti has notable effects on electrical conductivity, but the effects of Ti is different between the H-rich and the H-poor regimes. In the H-rich regime, electrical conductivity of olivine is weakly dependent on Ti content but has different sensitivity to water content than a Ti-poor olivine. In contrast, in the H-poor regime, electrical conductivity of Ti-rich olivine is substantially higher than the conductivity of Ti-poor olivine. As a consequence, the effect of hydrogen for the Ti-rich synthetic olivine on electrical conductivity is smaller than for the Ti-poor (natural) olivine for the modest H content expected in the asthenosphere, whereas in the H-poor lithosphere Ti will enhance the electrical conductivity substantially. Possible models to explain these observations are proposed including the interaction of Ti-related defects and H-related defects as well as the charge transfer caused by the hopping conduction due to $Ti^{3+} \Leftrightarrow Ti^{4+}$ under the H-poor conditions. We conclude that the addition of Ti to olivine affects the behavior of H-related defects, and therefore the applications of results from Ti-rich olivine samples to the Ti-poor real Earth need to be made with great care.

1. Introduction

The role of hydrogen to enhance many defect-related properties such as high-pressure experiments from the electrical conductivity and plastic deformation in olivine is well established (e.g., Dai et al., 2020; Karato, 2019; Karato & Jung, 2003; Karato & Wang, 2013; Mei & Kohlstedt, 2000a, 2000b). A large number of previous investigations are mainly focused on the effects of hydrogen on high-pressure physical properties of olivine, and the influence of impurities other than hydrogen has not been studied in any detail. However, a series of papers suggested the importance of some charged impurities such as Ti on hydrogen dissolution in olivine (e.g., Berry et al., 2005; Tollan et al., 2017, 2018). In particular, Cline et al. (2018) reported that in Ti-doped olivine, hydrogen has little effect on anelasticity. This is a puzzling observation because anelasticity is closely linked to plastic flow (e.g., Karato, 2008; McCarthy et al., 2011), and hence one expects some influence of hydrogen on anelasticity (e.g., Karato, 2012).

As is well known in semiconductor physics (e.g., Kittel, 1986; Phillips, 1973), addition of charged impurities (ionic species with electric charge that is different from the charges of ions in the host material) can modify defect-related properties substantially. Therefore, when charged defects other than hydrogen (e.g., Ti^{4+}) are present, the influence of hydrogen on physical properties might be modified. Consequently, it is not clear if the role of hydrogen in olivine is similar between a sample with the low TiO_2 content (most of natural olivine has 10–100 ppm wt of TiO_2; e.g., De Hoog et al., 2010) and a sample with the high TiO_2 content used in some experimental studies (Cline et al., 2018, used samples with the TiO_2 content up to 800 ppm wt).

In this study, we investigate the influence of Ti and H dissolution on electrical conductivity of olivine. We used synthetic samples with a range of TiO_2 content from 200 to 683 ppm wt (TiO_2) with varying H content. We will report the results, provide possible models to explain new observations, and discuss the roles of Ti on electrical conductivity in the upper mantle. Finally, some possible implications of Ti on other physical properties such as seismic attenuation and high-temperature creep will be discussed.

Table 1
A Summary of Chemical Composition of Dry and Hydrous Ti-Bearing Synthetic Olivine

Run no.	MgO (wt%)[a]	FeO (wt%)[a]	SiO_2 (wt%)[a]	X_{Ti} (ppm)[b]	C_w (wt%)
K1997	49.35	9.77	40.87	200	0.055
K1998	49.35	9.77	40.87	200	0.024
K2004	49.35	9.77	40.87	200	0.0070
K2007	49.35	9.77	40.87	683	0.053
K2008	49.35	9.77	40.87	683	0.021
K2009	49.35	9.77	40.87	683	0.0076
K2016	49.35	9.77	40.87	683	0.0011
K2017	49.35	9.77	40.87	683	0.046
K2020	49.35	9.77	40.87	683	0.044
K2019	49.35	9.77	40.87	683	0.0013
K2022	49.35	9.77	40.87	683	0.0012

[a]The content of these oxides are based on the composition of the starting materials ($[(Mg_{0.9},Fe_{0.1})_2SiO_4]$) by virtue of the sol-gel synthetic method. [b]The corresponding Ti contents are obtained from individual samples using ICP-MS analysis in the Department of Earth and Planetary Sciences, Yale University.

2. Hydrogen-Related Defects in Olivine

In most minerals, some mount of hydrogen can be dissolved as point defects (e.g., Karato, 2008). In case of "pure" $(Mg,Fe)_2SiO_4$ olivine, likely mechanisms of hydrogen dissolution are dissolution at cation sites, for example, $(2H)_M^{\times}$ or $(4H)_{Si}^{\times}$ in addition to other ionized defects (e.g., Karato, 2008; Kohlstedt et al., 1996). However, the role of other charged impurities such as Ti^{4+} and Cr^{3+} on the dissolution of hydrogen has also been suggested (e.g., Berry et al., 2005; Berry, O'Neil, et al., 2007; Berry, Walker, et al., 2007; Tollan et al., 2017, 2018).

Hydrogen (H) enhances electrical conductivity in olivine via diffusion of some H-related defects (e.g., Karato, 1990, 2019; Yoshino & Katsura, 2013). However, experimental studies also show that there are multiple H-related defects whose concentration and mobility are different that makes a complication including the changes in conductivity anisotropy with temperature (e.g., Dai & Karato, 2014a; Karato, 2015). Similarly, hydrogen enhances plastic deformation and grain growth presumably through some H-related defects (e.g., Karato, 1989; Karato & Jung, 2003; Mei & Kohlstedt, 2000a, 2000b).

Ti and hydrogen may be dissolved in olivine as (e.g., Tollan et al., 2017)

$$TiO_2 + H_2O + \text{olivine} = \left[Ti_M^{\bullet\bullet} + (2H)_{Si}^{''}\right]_{\text{olivine}} + MgSiO_3 \quad (1)$$

where the Kröger-Vink notation of point defects is applied, and a symbol $\left[Ti_M^{\bullet\bullet} + (2H)_{Si}^{''}\right]_{\text{olivine}}$ indicates olivine containing a pair of defects $Ti_M^{\bullet\bullet}$ and $(2H)_{Si}^{''}$. Evidence of such a mechanism was presented by Berry, Walker, et al. (2007). In this case, Ti and H would interact strongly, and the mobility of hydrogen might be different from a case where Ti content is less. In order to test this hypothesis, we investigated electrical conductivity of olivine where both hydrogen and Ti (TiO_2) are dissolved.

3. Experimental Procedure

3.1. Sample Preparation and Characterization

In the present study, we used a sol-gel method to synthesize the high-purity olivine $[(Mg_{0.9},Fe_{0.1})_2SiO_4]$ with the TiO_2 content of 200 and 700 ppm wt following the method by Faul and Jackson (2007). We produced synthetic olivine of composition $(Mg_{0.9}Fe_{0.1})_2SiO_4$ + 200 and 683 ppm wt TiO_2 (see Table 1) with ~2% excess orthopyroxene. Powder samples are annealed for 18 hr in the furnace at the predesigned temperature of 1573 K, where the oxygen partial pressure is controlled by the Ar + H_2/CO_2 mixed gas to achieve the oxygen fugacity of sample chamber close to the Ni–NiO buffer.

In order to explore the influence of oxygen fugacity on electrical conductivity, we prepared samples synthesized using three different solid oxygen buffers (e.g., Re–ReO_2, Ni–NiO, and Mo–MoO_2). The synthesis experiments were conducted at high P and T (P = 4 GPa and T = 1373 K) for 3 hr.

To add water (hydrogen), high-pressure annealing experiments were performed at the pressure of 4.0 GPa and temperature of 1373 K, where the annealing time is 3 hr and the oxygen partial pressure in sample chamber is controlled using the double layers of nickel capsule. A mixture of talc and brucite (6:1 weight ratio) was used as a water resource. In order to prepare samples with smaller water content, we remove water from those samples by heating under water-poor conditions in the high-temperature furnace. These drying experiments were made at 873 K using different annealing time of 1.0, 3.0, and 7.0 hr using the Ar + H_2/CO_2 mixed gas to control the oxygen partial pressure near the Ni–NiO buffer.

Water (hydrogen) in samples was investigated using Fourier transform infrared (FT-IR) spectroscopy both before and after the conductivity measurements. FT-IR absorption spectra were taken from approximately five locations in a sample using 100 μm aperture for the wavenumber of 1,000–4,000 cm^{-1} using Varian

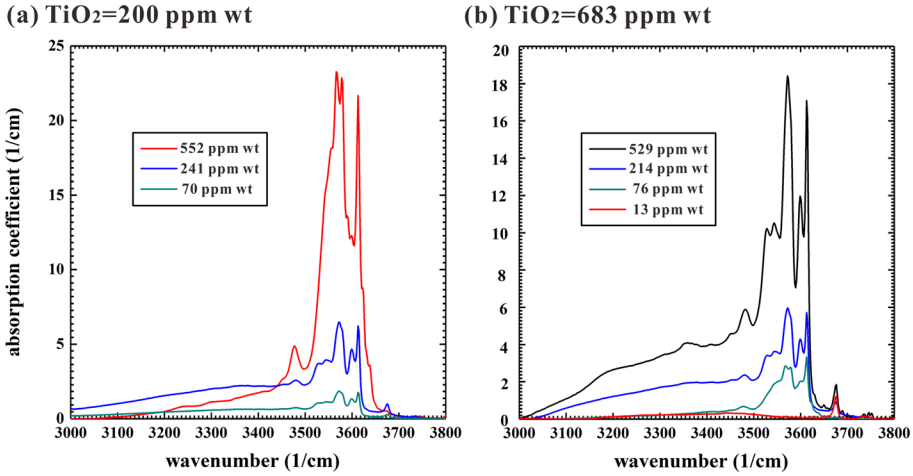

Figure 1. The representative FT-IR spectra of synthetic olivine aggregates with the TiO_2 content of 200 ppm wt (a) and 683 ppm wt (b) for the wavenumber range of 3,000–3,800 cm^{-1}. For each sample, the highest water content corresponds to the starting sample. Each starting sample was dried to remove water content. We measured electrical conductivity for each sample (a total of seven) (we also took FT-IR spectra for each sample before and after each conductivity measurement. The difference in FT-IR absorption is small (less than ~7% between before and after).

UMA FT-IR microscope. The sample is ~200 μm thick, and for each measurement we took 128 scans. For each sample, FT-IR measurements were made on five different regions. We report the average and standard deviation from these measurements. FT-IR absorption spectra of all the samples are shown in Figure 1. The difference in water content between before and after conductivity measurement is less than 7%.

The Paterson (1982) equation was chosen to calculate the water content of sample:

$$C_{OH} = \frac{B_i}{150\xi}\int \frac{K(v)}{(3,\ 780 - v)}dv \quad (2)$$

where C_{OH} is the molar concentration, B_i is the density factor of olivine, ξ is the orientational factor, and K (v) is the absorption coefficient. Integration was made from 3,000 to 3,750 cm^{-1} (if the Bell calibration, Aubaud et al., 2009; Bell et al., 2003, is employed, ~3 times higher water content will be obtained).

The water content of the initial hydrothermally prepared samples is ~550 ppm wt (8,600 H/10^6Si H_2O) for a sample with 200 ppm wt TiO_2, and 530 ppm wt (8,200 H/10^6Si H_2O) for a sample with 683 ppm wt TiO_2, respectively. After annealing the sample in the furnace at temperature of 873 K and atmospheric pressure, water content of sample was reduced accordingly, as shown in Table 1. Room pressure annealing reduces the total water content, but the relative intensity of absorption at various frequencies does not change so much by room pressure annealing. The relative uncertainties in water content measurement depend on the water content and is ~10–20% for water-rich sample (a sample with ~550 ppm wt water) but is larger (~50%) for a water-poor sample (a sample with ~13 ppm wt water).

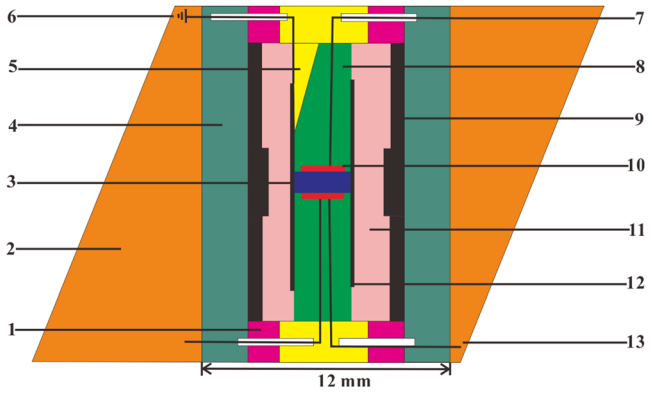

Figure 2. Experimental assemblage for electrical conductivity measurements of olivine aggregates in the Kawai-1000t multianvil press: (1) a metallic Mo ring; (2) MgO octahedral pressure medium with its edge length of 25 mm; (3) a sample; (4) zirconia; (5) Al_2O_3 insulation cement; (6) an electric grounding; (7) a lead wire of metallic electrode and Al_2O_3 insulation tube; (8) an insulation tube made of four-hole alumina; (9) a heater of lanthanum chromite; (10) two symmetric buffer electrodes; (11) an MgO insulation tube; (12) a metallic shielding case made of Ni, Re, or Mo foil; and (13) a thermocouple and Al_2O_3 insulation tube.

3.2. Methods of Conductivity Measurements

Experimental assemblage for electrical conductivity measurements of olivine aggregates in the Kawai-1000t multianvil press is shown in Figure 2. Sample assembly with its dimension of "25 × 17" was symmetrically installed in the cubic anvil of tungsten carbide, which the edge length

Table 2
Summary of Run Conditions and the Water Content of the Samples

Run no.	X_{Ti} (ppm)	P (GPa)	T (K)	Oxygen buffers	Water content			
					Before experiment		After experiment	
					ppm wt	H/10^6 Si	ppm wt	H/10^6 Si
K1997	200	4	873–1273	Ni–NiO	552 ± 10	8,592 ± 161	551 ± 9	8,589 ± 142
K1998	200	4	873–1273	Ni–NiO	241 ± 13	3,748 ± 206	240 ± 14	3,747 ± 225
K2004	200	4	873–1273	Ni–NiO	70 ± 10	1,072 ± 159	68 ± 12	1,067 ± 192
K2007	683	4	873–1273	Ni–NiO	529 ± 12	8,231 ± 188	527 ± 14	8,209 ± 217
K2008	683	4	873–1273	Ni–NiO	214 ± 20	3,323 ± 331	212 ± 15	3,296 ± 234
K2009	683	4	873–1273	Ni–NiO	76 ± 17	1,182 ± 269	75 ± 13	1,164 ± 206
K2016	683	4	873–1273	Ni–NiO	13 ± 5	199 ± 75	9 ± 3	132 ± 40
K2017	683	4	873–1273	Re–ReO_2	458 ± 7	7,131 ± 109	456 ± 10	7,110 ± 162
K2020	683	4	873–1273	Mo–MoO_2	435 ± 11	6,760 ± 173	433 ± 12	6,733 ± 193
K2019	683	4	873–1273	Re–ReO_2	13 ± 6	186 ± 81	10 ± 4	163 ± 70
K2022	683	4	873–1273	Mo–MoO_2	12 ± 4	184 ± 65	10 ± 5	160 ± 79

for the octahedral pressure medium of magnesium oxide and the magnitude of truncation for the cubic tungsten carbide anvil is 25 mm and 17 mm, respectively. Pressure is calibrated by virtue of the phase transition of some representative minerals at high-temperature and high-pressure conditions, such as quartz and olivine (Morishima et al., 1994; Zhang et al., 1996). Before each electrical conductivity measurement, all parts in the electrical conductivity assembly were baked 12 hr at 1223 K in the muffle furnace so as to remove the adsorbed water. The metallic foil shield is installed between the sample and the insulating tube of magnesium oxide to minimize the electric noise from the heater. Material for the shield is the same metal as the metal used to synthesize the sample. One disc-shaped olivine sample that is obtained using the ultrasonic core sampling equipments with several different sizes of diamond drilling tools was switched into two symmetric electrodes where the insulation ring of alumina was surrounded. The electrode material is the same metal as used to synthesize the sample. The thermocouple of $W_{5\%}Re$–$W_{26\%}Re$ was adopted to monitor the experimental temperature during the process of electrical conductivity measurements. The experimental uncertainties from the fluctuations of the respective pressure and temperature are less than 0.5 GPa and 10 K. The measurement uncertainty from the analysis of fitted impedance spectroscopy in sample is no more than less than 3%.

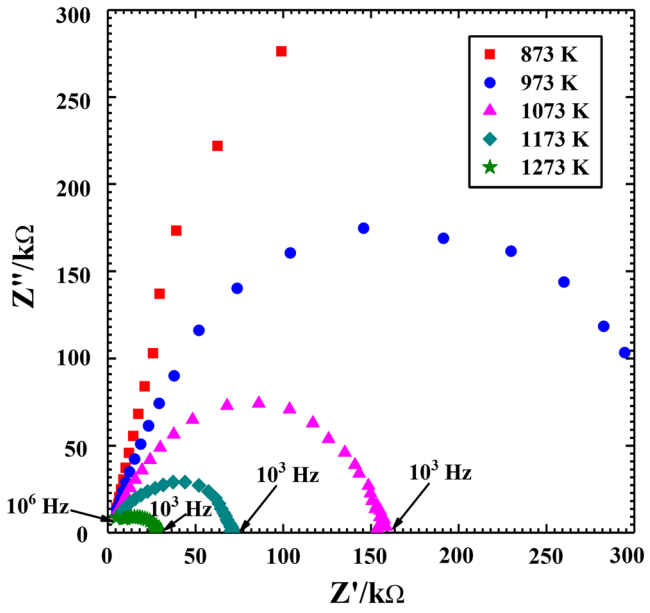

Figure 3. The Z′ (real part of the impedance) versus Z″ (imaginary part of the impedance) plot of complex impedance spectra of synthetic olivine aggregates with TiO_2 content of 683 ppm wt from 10^3–10^6 Hz (right to left), obtained under conditions of 4 GPa, 873–1273 K, the Ni–NiO oxygen buffer, and the water content of ~214 ppm wt.

For each electrical conductivity measurements, the pressure was increased with a rate of ~1.0 GPa/hr to 4.0 GPa. After the pressure reached 4.0 GPa, the temperature was gradually increased with a rate of ~80 K/min up to the predetermined value. Then, the complex impedance spectroscopy of a sample was made at a given temperature and pressure. After completing the impedance spectroscopy at a given temperature (at 4 GPa), we changed temperature and other impedance spectroscopy measurements were made at a different temperature. Grain size of our samples was determined by scanning electron microscope (SEM) observations. It is ~10 ± 5 μm before and after each electrical conductivity measurements.

The impedance spectroscopy was made using the Solartron 1260 for the frequency range of 10^3–10^6 Hz (we choose relative high-frequency range to minimize the water loss; see Karato, 2019) and the signal voltage is 1.0 V. In the impedance spectroscopy, we determine both the in-phase and out-of-phase response of a sample to the applied AC voltage. Measuring both in-phase (real part of impedance [Z′]) and out-of-phase (imaginary part of impedance [Z″]) response is important because when conduction is due to migration of ions, migrating ions can be accumulated at the

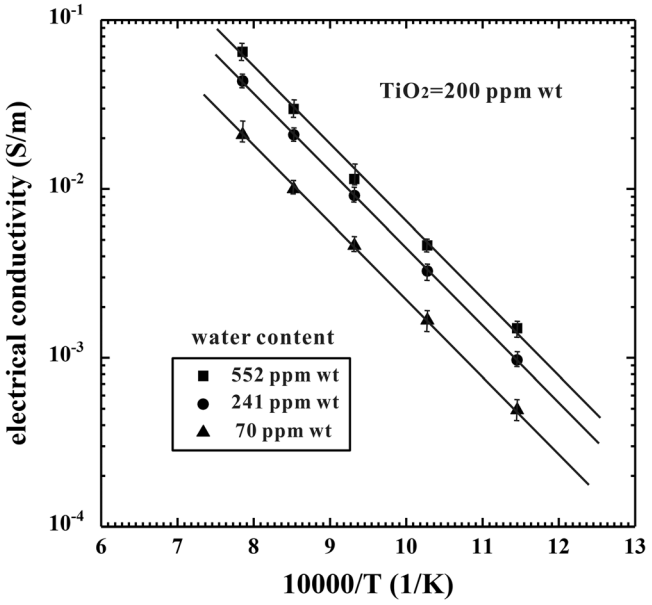

Figure 4. Electrical conductivity versus inverse temperature relationship of synthetic olivine aggregates with TiO_2 content of 200 ppm wt at 4 GPa, 873–1273 K, and the Ni–NiO oxygen buffer.

electrode (or at grain boundaries) that prevents the migration of other ions. In most cases, the electrical conductivity of sample was acquired during the first cycle of decreasing temperature after the peak temperature was reached. The experimental conditions are summarized in Table 2.

Figure 3 shows typical impedance spectroscopy results for the synthetic olivine aggregates with the Ti-bearing content of 683 ppm wt under conditions of 4 GPa, 873–1273 K, the Ni–NiO oxygen buffer, and the ~214 ppm wt of water content. Other impedance spectra on Ti-bearing olivine aggregates acquired under the conditions of different temperature, oxygen fugacity, and water content are similar to these results. We observe clearly defined half circle which implies the equivalent circuit characterizing the sample behavior is a parallel connection of resistor and capacitor (Barsoukov & Macdonald, 2005; Roberts & Tyburczy, 1993). Using such a model, we determined the resistance of a sample (R).

The electrical conductivity of a sample was calculated from the determined resistivity and the geometry of a sample using

$$\sigma = \frac{L/S}{R} = \frac{L}{SR} \tag{3}$$

where L is the thickness of a sample and S is the cross-sectional area of the electrode. Before and after each electrical conductivity measurements, both of the sample thickness and the cross-sectional area of the metallic electrode were measured. The uncertainties in the calculated conductivity caused by the uncertainties in the sample geometry are less than ~5%.

We used the following equation to fit the data:

$$\sigma = A_{\text{anhdrous(hydrous)}} \left(\frac{f_{O_2}}{f_{O_20}}\right)^{q_{\text{anhydrous}}} \exp\left(-\frac{H^*_{\text{anhydrous}}}{RT}\right) + A_{\text{hydrous}} \left(\frac{C_W}{C_{W0}}\right)^{r} \left(\frac{f_{O_2}}{f_{O_20}}\right)^{q_{\text{hydrous}}} \exp\left(-\frac{H^*_{\text{hydrous}}}{RT}\right) \tag{4}$$

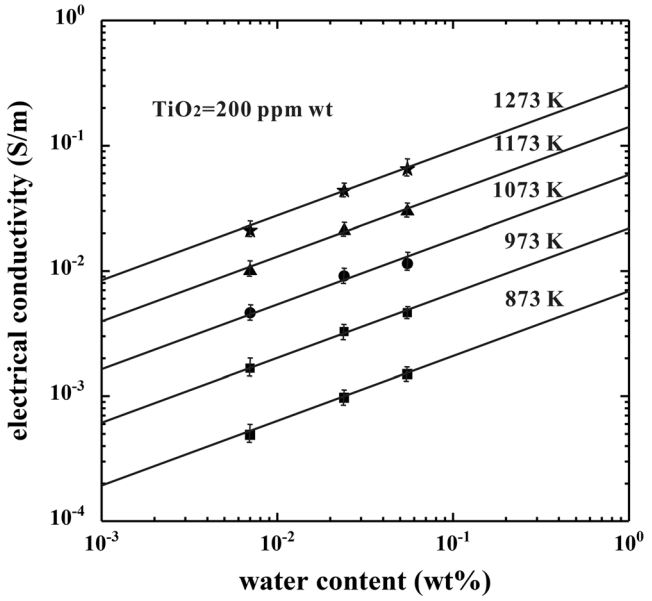

Figure 5. Electrical conductivity-water content relationship of synthetic olivine aggregates with TiO_2 content of 200 ppm wt at 4 GPa for the Ni–NiO oxygen buffer for different water contents, showing $\sigma \propto C_W^r$ with $r = 0.51 \pm 0.18$ (C_W = water content).

where $A_{\text{anhdrous(hydrous)}}$ is the preexponential factor of anhydrous (hydrous) olivine (S/m), $H^*_{\text{anhydrous(hydrous)}}$ is the activation enthalpy of anhydrous (hydrous) sample (kJ/mol), f_{O_2} is oxygen fugacity, $q_{\text{anhydrous(hydrous)}}$ is a constant characterizing the oxygen fugacity dependence, f_{O_20} is the reference oxygen fugacity of the Ni–NiO oxygen buffer, C_W is the water content, C_{W0} is a reference water content (= 0.01 wt%), r is a constant characterizing the water content dependence, T is the absolute temperature (kelvin), and R is the gas constant. To estimate these parameters, we use our new data as well as some of the previous results for smaller TiO_2 content (e.g., San Carlos olivine, Wang et al., 2006 [for wet olivine], Xu et al., 2000 [for dry olivine], and synthetic olivine without TiO_2, Dai & Karato, 2014b). Our data set is limited, and therefore we cannot determine all of these parameters, but we can get reasonable constraints on the conduction mechanism of Ti-bearing olivine.

4. Results

The results including the effects from the variations of water content and oxygen fugacity on electrical conductivities of Ti-bearing olivine can be summarized in Figures 4–8 and Tables 3–6.

For the Ni–NiO oxygen buffer, the dependence relations between the electrical conductivity of olivine with its correspondent Ti-bearing content of ~200 ppm wt on the temperature/water content at 4 GPa are displayed in

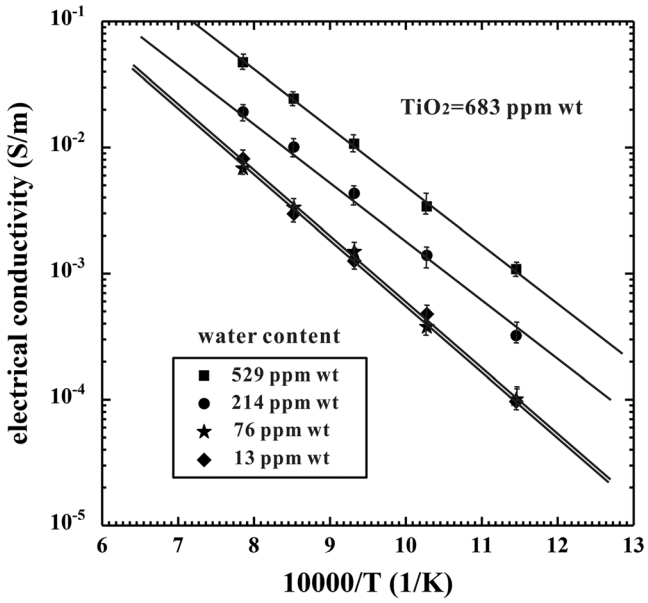

Figure 6. Electrical conductivity versus inverse temperature relationship of synthetic olivine aggregates with TiO_2 content of 683 ppm wt at 4 GPa, 873–1273 K, and the Ni–NiO oxygen buffer.

Figures 4 and 5. It makes clear that at lower Ti-bearing synthetic olivine (~200 ppm wt), the electrical conductivity of sample will tend to increase with the rise of water content. The water content sensitivity parameter r is determined to be $r = 0.51 \pm 0.18$ (C_W = water content) for a sample with TiO_2 200 ppm wt. Figures 6 and 7 illustrate the dependence relations of the electrical conductivity of olivine with its correspondent Ti-bearing content of ~683 ppm wt on the temperature and water content at 4 GPa. It can be seen clearly that a similar tendency was also observed for the Ti-rich synthetic olivine aggregates (TiO_2 = 683 ppm wt) and showed more strong dependent relation of electrical conductivity of Ti-rich

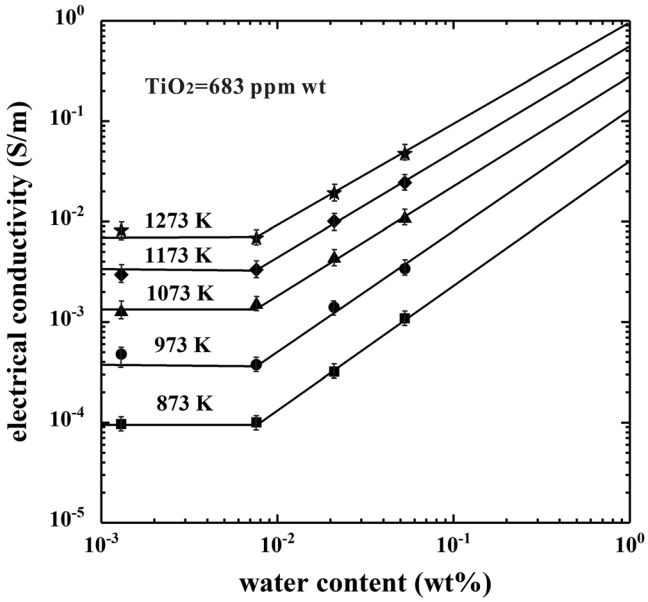

Figure 7. Electrical conductivity versus water content relation for hydrous synthetic olivine aggregates with TiO_2 content of 683 ppm wt under conditions of 4 GPa, 873–1273 K, and the Ni–NiO oxygen buffer, showing $\sigma \propto C_W^r$ with $r = 0.98 \pm 0.21$ (C_W = water content) for $C_w > 10^{-2}$ ppm wt, but below this, conductivity is nearly independent of water content.

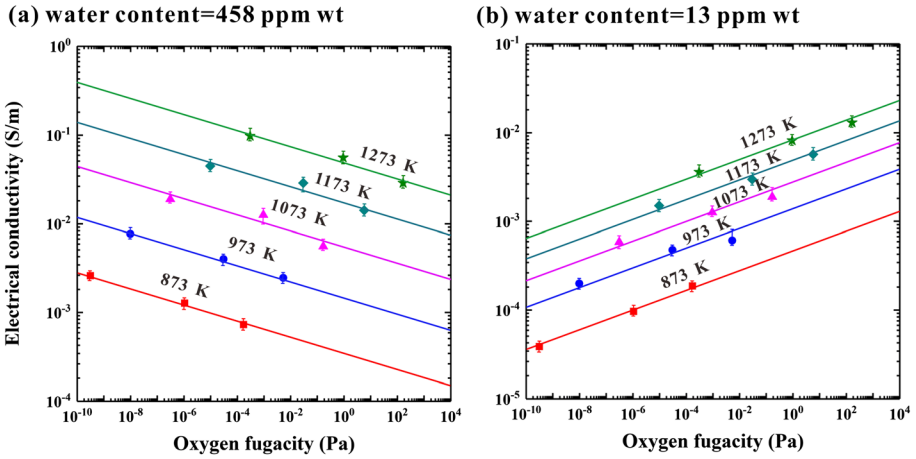

Figure 8. Influence of oxygen fugacity on the electrical conductivity of (a) hydrous (water content = 458 ppm wt) and (b) anhydrous (water content = 13 ppm wt) olivine aggregates with TiO_2 content of 683 ppm wt under conditions of 4.0 GPa and 873–1273 K for three different solid buffers (e.g., Mo–MoO_2, Ni–NiO, and Re–ReO_2).

olivine on water content at the condition of water content larger than ~7.6×10^{-3} wt% ($r = 0.98 \pm 0.21$). However, a relatively stable electrical conductivity for Ti-rich olivine aggregates was observed and displayed a nondependence of electrical conductivity of sample on the variation of water content at the water-poor regime (its water content ranges from ~10^{-3} to ~7.6×10^{-3} wt%). Obviously, the activation enthalpy of Ti-rich and water-rich olivine (ΔH) is lower than the value of dry Ti-bearing sample; however, the activation enthalpy of dry Ti-bearing olivine is lower than previously published Ti-free synthetic olivine (Dai & Karato, 2014b). The fitted parameter results of electrical conductivity for the Ti-bearing olivine are list in Tables 3 and 4.

The dependence relations between the electrical conductivity of dry and hydrous olivines with Ti-bearing content of ~683 ppm wt on the oxygen fugacity are shown in Figure 8 and Table 5 at 4 GPa, 873–1273 K, 458 ppm wt water, and controlled oxygen fugacities using three different solid oxygen buffers (e.g., Re–ReO_2, Ni–NiO, and Mo–MoO_2) at 4.0 GPa and 873–1273 K. The water content in hydrous Ti-rich sample is 458 ppm wt, and the oxygen fugacity is controlled by using three different solid oxygen buffers (e.g., Re–ReO_2, Ni–NiO, and Mo–MoO_2).

Further, the average exponential factor of oxygen fugacity (q) that can be used to describe the dependence relation of electrical conductivity on the oxygen fugacity for dry and wet olivine are 0.097 ± 0.008 and -0.089 ± 0.006, respectively, which are close to those obtained q values of dry and wet olivine results of 0.096 and −0.066, respectively (Dai et al., 2010; Dai & Karato, 2014c). In addition, for each correspondent temperature point, our present obtained dependence relations between the electrical conductivity on the variation of oxygen fugacity are shown in Table 6. It is clear that the absolute terms of q reduce with the rise of temperature.

Table 3
Fitted Parameters of Arrhenius Relation for the Electrical Conductivity of Ti-Bearing Hydrous Olivine Under Conditions of 4.0 GPa, 873–1273 K, and the Ni–NiO Oxygen Buffer

Run no.	X_{Ti} (ppm)	C_w (wt%)	Log σ_0	H^* (kJ mol^{-1})
K1997	200	0.055	2.34 ± 0.08	87 ± 2
K1998	200	0.024	2.24 ± 0.12	89 ± 3
K2004	200	0.0070	1.86 ± 0.09	87 ± 2
K2007	683	0.053	2.32 ± 0.05	89 ± 2
K2008	683	0.021	2.21 ± 0.03	96 ± 4
K2009	683	0.0076	1.92 ± 0.06	100 ± 3
K2016	683	0.0013	1.99 ± 0.04	101 ± 2

Table 4
Fitted Parameter Values for Electrical Conductivity of Hydrous and Anhydrous Synthetic Ti-Bearing Olivine Aggregates Under Conditions of 4.0 GPa, 873–1273 K, and Oxygen Fugacity Controlled by Three Oxygen Buffers (Mo–MoO_2, Ni–NiO, and Re–ReO_2)

X_{Ti} (ppm)	Water-bearing conditions	Oxygen buffers	Log_{10} [A (S m^{-1})]	r	q	H^* (kJ mol^{-1})
200	Hydrous	Ni–NiO	3.01 ± 0.32	0.51 ± 0.18	–	87 ± 3
683	Hydrous	Mo–MoO_2, Ni–NiO and Re–ReO_2	3.98 ± 0.19	0.98 ± 0.21	−0.089 ± 0.006	94 ± 2
683	Anhydrous	Mo–MoO_2, Ni–NiO and Re–ReO_2	1.94 ± 0.13	–	0.097 ± 0.008	100 ± 2

5. Discussions

Our results show that the addition of Ti (TiO_2) has a marked effect when TiO_2 content exceeds ~200 ppm wt, but the effects of Ti are different between the H-poor and the H-rich regimes. This is shown in Figure 9 where we plot electrical conductivity of olivine with different TiO_2 content (683 and ~30 ppm wt (San Carlos olivine)) as a function of water content. The comparison is made at $P = 4$ GPa and $T = 1073$ K for the oxygen fugacity corresponding to the Ni–NiO buffer. Results for San Carlos olivine are from Wang et al. (2006) for wet conditions and from Xu et al. (2000) for dry conditions.

In the present studies, we found that one markedly different electrical transport behavior in the Ti-poor and Ti-rich olivines was observed at the respective water-poor ("dry") and the water-rich ("wet") regimes. In the "dry" regime, electrical conductivity of Ti-rich olivine is much higher than that of Ti-poor olivine. In contrast, for the "wet" regime (water content >100 ppm wt), the influence of Ti is smaller, and a comparison of results for samples with different Ti content needs to be done carefully. In our experiments, we prepared two samples with different TiO_2 content using the same method (sol-gel synthesis), we focus on those two sets of the results seen in Figure 10. From such a comparison, we conclude that the water content dependence (parameter "r" in Equation 4) is different between Ti-poor sample and Ti-rich sample.

In Ti-poor hydrogen-doped olivine such as San Carlos olivine, hydrogen-assisted electrical conduction is caused by the migration of interstitial (or "free") proton at relatively low temperature ($T < 1300$ K) (e.g., Dai & Karato, 2014c; Karato, 2015, 2019; Karato & Wang, 2013). The value of "r" for such a model is 1/2–3/4 that is consistent with the experimental observations. When Ti is doped, the value of "r" is ~1, and as a result, conductivity is substantially smaller than that for a Ti-poor olivine at relatively water-poor conditions (Figure 10). In Ti-rich olivine, hydrogen may be incorporated in combination of Ti at M site, the charge balance being maintained by $\left[\text{Ti}_M^{\bullet\bullet}\right] = \left[(2\text{H})^{''}_{\text{Si}}\right]$ (e.g., Berry, Walker, et al., 2007). When hydrogen is trapped at the Si site, ionization of hydrogen to produce interstitial hydrogen will be difficult. In such a case, electrical conductivity is less than a case of hydrated olivine with small or no Ti. And this model predicts $\left[(2\text{H})^{''}_{\text{Si}}\right] \propto f_{H_2O} \propto C_W$ ($r = 1$). Therefore, if hydrogen in $(2\text{H})^{''}_{\text{Si}}$ contributes to electrical conductivity, the water content exponent will be $r = 1$. In its simplest version, this model predicts that conductivity is insensitive to oxygen fugacity. The observed small negative dependence relation of electrical conductivity on the variation of oxygen fugacity implies that we need to invoke a modified model. One possibility is to assume that some Ti is

Table 5
The Fitted Parameters of Arrhenius Relation for Hydrous and Anhydrous Synthetic Olivine Aggregates With Its Ti Content of 683 ppm wt Under Conditions of 4.0 GPa and Oxygen Fugacity Controlled by Three Oxygen Buffers (Mo–MoO_2, Ni–NiO, and Re–ReO_2)

Samples	Oxygen buffers	T (K)	$\text{Log}_{10}\,\sigma_0$ (S/m)	H^* (kJ/mol)	Average q
Hydrous (all data)	Re–ReO_2	873–1273	1.90 ± 0.15	85 ± 2	
	Ni–NiO	873–1273	2.39 ± 0.17	89 ± 5	−0.089 ± 0.006
	Mo–MoO_2	873–1273	2.37 ± 0.12	84 ± 3	
Anhydrous (all data)	Re–ReO_2	873–1273	2.14 ± 0.19	100 ± 6	
	Ni–NiO	873–1273	1.95 ± 0.08	100 ± 2	0.097 ± 0.008
	Mo–MoO_2	873–1273	1.79 ± 0.09	104 ± 3	

Note. The fitted parameters, σ_0 and H^* correspond to our synthetic sample with the Ti content of 683 ppm wt (The standardized water content of 458 ppm wt was determined by the Paterson calibration).

Table 6
The Fitted Parameters of Arrhenius Relation for Hydrous (~458 ppm wt) and Dry (~10 ppm wt) Synthetic Olivine Aggregates With Its Ti Content of 683 ppm wt Under Conditions of 4.0 GPa and Controlled Oxygen Buffers (Re–ReO_2, Ni–NiO, and Mo–MoO_2)

	T	q
Wet (All data)	873	−0.096 ± 0.002
	973	−0.091 ± 0.005
	1073	−0.089 ± 0.001
	1173	−0.088 ± 0.002
	1273	−0.084 ± 0.004
Dry (All data)	873	0.120 ± 0.002
	973	0.099 ± 0.003
	1073	0.098 ± 0.002
	1173	0.089 ± 0.002
	1273	0.087 ± 0.001

dissolved in olivine as Ti^{3+}, say $Ti_M^{\bullet}$. In this case, the charge balance will be $\left[Ti_M^{\bullet}\right] = \left[(3H)_{Si}^{'}\right]$. Since $\left[Ti^{3+}\right] \propto f_{O_2}^{q}$ with $q < 0$, this explains the observed fO_2 dependence.

The observed FT-IR absorption spectra of olivine with different TiO_2 content could potentially provide some hint on the nature of hydrogen-related defects in these samples. However, the differences in FT-IR spectra among olivine with different TiO_2 content are minor: In all samples, dominant absorption peaks are located at 3,525–3,610 cm^{-1}. And the assignment of absorption peaks to specific hydrogen-related defects is unclear. For example, although Tollan et al. (2017) proposed that absorption peaks at 3,525 and 3,572 cm^{-1} are due to Ti-related hydrogen defects, strong absorption peaks at/or near these frequencies are observed in Ti-poor olivine (Ti-bearing olivine in this study and San Carlos olivine) where molar concentration of H determined by the IR absorption far exceeds that of Ti. Consequently, we consider that the correspondence for IR peaks with H speciation is not well understood at this time, and we do not use FT-IR spectra to discuss the model of electrical conductivity in this paper.

In the water-poor regime (i.e., "dry" conditions), electrical conductivity in Ti-poor olivine is considered to be due to the charge transfer between $Fe^{2+} \Leftrightarrow Fe^{3+}$(e.g., Karato, 1974; Schock et al., 1989). The evidence for this is the positive dependence of electrical conductivity on oxygen fugacity. In Ti-rich olivine, oxygen fugacity dependence of electrical conductivity in the "dry" regime is similar to that of Ti-poor olivine, but the magnitude of conductivity is much higher than that of Ti-poor olivine. Also, the activation energy of conductivity in Ti-rich sample in the "dry" regime (~100 kJ/mol) is substantially lower than that of Ti-poor olivine (~130–150 kJ/mol). Consequently, we conclude that electrical conductivity in Ti-rich "dry" olivine is due to something other than the charge transfer between $Fe^{2+} \Leftrightarrow Fe^{3+}$. One possible mechanism is charge transfer

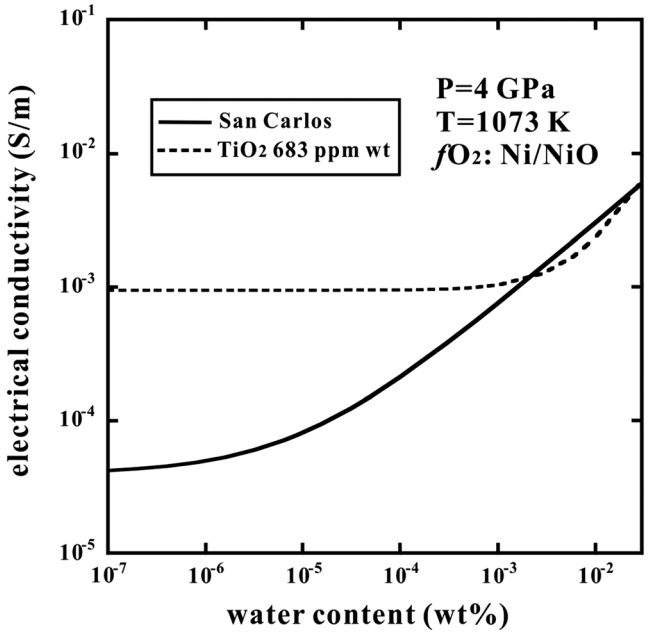

Figure 9. Electrical conductivity of Ti-poor (San Carlos) olivine and Ti-rich (683 ppm wt) olivine as a function of water content (P = 4 GPa and T = 1073 K). The data for Ti-rich olivine is from the present study, and the data for San Carlos olivine is from Wang et al. (2006) (for water-rich conditions) and from Xu et al. (2000) (for water-poor conditions). The results of Wang et al. (2006) are under the water-rich conditions; the influence of Ti is small (but the water content dependence is different between Ti-poor and Ti-rich olivine; see also Figure 10). However, under the water-poor conditions, Ti enhances conductivity substantially.

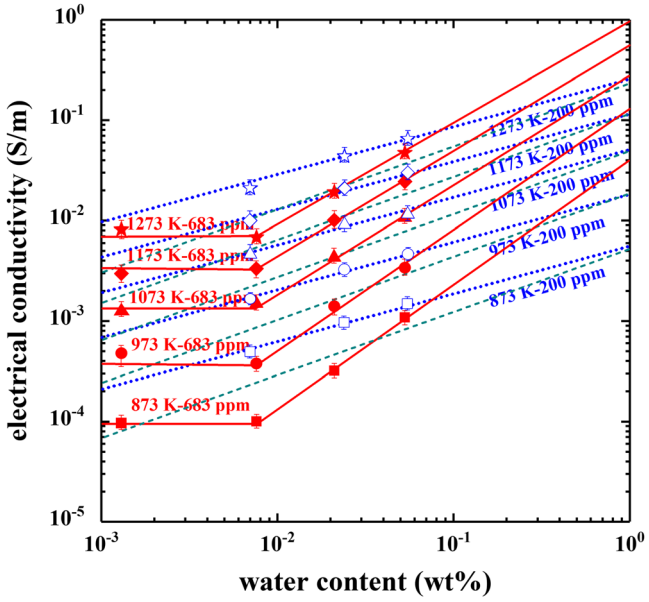

Figure 10. A comparison of two samples with different Ti content from this study and previous conductivity results of hydrous San Carlos olivine. The blue dot, red solid, and green dash lines are for samples with 200 and 683 ppm wt TiO_2 in the present studies and hydrous San Carlos olivine by Wang et al. (2006).

between $Ti^{3+} \Leftrightarrow Ti^{4+}$ in analogy with $Fe^{2+} \Leftrightarrow Fe^{3+}$. In order for this model to work, it must satisfy the relation of $[Ti^{3+}] > [Ti^{4+}]$, but the validity of this notion needs to be tested. Also, the quantitative relationship between TiO2 content and conductivity needs to be constrained better.

6. Summary and Conclusions

We measured electrical conductivity of H (hydrogen) and Ti (titanium) doped olivine to understand how Ti modifies the mobility and concentration of charged defects in olivine. Doping of Ti modifies electrical conductivity of olivine differently between water (H)-rich and water (H)-poor regimes: In the water-poor regime, addition of Ti increases electrical conductivity substantially, whereas in the water-rich regime, addition of Ti has smaller effects on conductivity, but it changes the water content sensitivity suggesting a change in the mechanism of conductivity. In contrast, oxygen fugacity dependence of electrical conductivity of Ti-doped samples is similar to that of Ti-poor samples: In both samples, electrical conductivity increases with oxygen fugacity in the H-poor regime, whereas it decreases with oxygen fugacity in the water-rich regime. In most of the asthenosphere, hydrogen content far exceeds Ti content, and therefore the role of Ti is likely negligible. In contrast, in the water-poor regions such as in the lithosphere Ti may play an important role. Because the magnitude of TiO2 effect in the "dry" regime is large, it is possible that some of the observed variations in electrical conductivity in the lithosphere may be due to the variation in TiO2 content. Further studies on this issue are warranted to understand the causes of heterogeneity of electrical conductivity in the lithosphere.

Our study shows that the addition of Ti modifies electrical conductivity of olivine substantially implying that the concentration and/or the mobility of charged point defects in olivine are affected by the addition of Ti. Because some other properties such as high-temperature creep and seismic attenuation are also related to defects, it is likely that the addition of Ti also modifies these properties.

However, published results on Ti and H effects on these properties are puzzling. Faul et al. (2016) investigated the influence of Ti and H doping on high-temperature creep in olivine and concluded that the creep strength of Ti- and H-doped olivine samples is reduced by the addition of hydrogen much the same way as has been shown in the previous results on Ti-poor but H-doped olivine (e.g., Karato et al., 1986; Mei & Kohlstedt, 2000a, 2000b). In contrast, Cline et al. (2018) conducted an experimental study on anelasticity in Ti- and H-doped olivine and reported that anelasticity is insensitive to hydrogen content. Given a close link between high-temperature creep and anelasticity (e.g., Karato, 2008; McCarthy et al., 2011), the contrasting reports by these studies are puzzling. Further studies are needed on the dissolution of hydrogen together with Ti and the influence of these defects on high-temperature creep and anelasticity in more systematic manner.

Acknowledgments

We are grateful to Ved Mittal for his kind assistance of sample preparation in Karato's high-pressure laboratory. We thank Haiying Hu, Jennifer Girard, Silber Reynold, Ved Mittal and Zhenting Jiang for helpful discussions. Professor Noah Planavsky kindly measured the TiO_2 content of our samples using ICP-MS analysis in the Department of Earth and Planetary Sciences, Yale University. This research was financially supported by the NSF of the United States (Grant No. EAR-1764271), Key Research Program of Frontier Sciences of CAS (Grant No. QYZDB-SSW-DQC009) of China and NSF of China (Grant Nos. 42072055, 41774099 and 41772042). The authors comply with AGU's data policy, and the data of this paper are available in Figshare (https://figshare.com/articles/dataset/Dai_and_Karato_Experimental_Data_xlsx/12941705). The authors declare no competing financial interests.

References

Aubaud, C., Bureau, H., Raepsaet, C., Khodja, H., Withers, A., Hirschmann, M., & Bell, A. (2009). Calibration of the infrared molar absorption coefficients for H in olivine, clinopyroxene and rhyolitic glass by elastic recoil detection analysis. *Chemical Geology*, *262*(1–2), 78–86. https://doi.org/10.1016/j.chemgeo.2009.01.001

Barsoukov, E., & Macdonald, J. R. (2005). *Impedance spectroscopy theory, experiment, and applications* (2nd ed., pp. 17–129). Hoboken, N. J: Wiley-Interscience.

Bell, D. R., Rossman, G. R., Maldener, J., Endisch, D., & Rauch, F. (2003). Hydroxide in olivine: A quantitative determination of the absolute amount and calibration of the IR spectrum. *Journal of Geophysical Research*, *108*(B2), 2105. https://doi.org/10.1029/2001JB000679

Berry, A. J., Hermann, J., O'Neill, H. S. C., & Foran, G. J. (2005). Fingerprinting the water site in mantle olivine. *Geology*, *33*(11), 869–872. https://doi.org/10.1130/G21759.1

Berry, A. J., O'Neil, H. S. C., Hermann, J., & Scott, D. R. (2007). The infrared signature of water associated with trivalent cations in olivine. *Earth and Planetary Science Letters*, *261*(1–2), 134–142. https://doi.org/10.1016/j.epsl.2007.06.021

Berry, A. J., Walker, A. M., Hermann, J., O'Neil, H. S. C., Foran, G. J., & Gale, J. D. (2007). Titanium substitution mechanisms in forsterite. *Chemical Geology*, *242*(1–2), 176–186. https://doi.org/10.1016/j.chemgeo.2007.03.010

Cline, C. J., Faul, U., David, E. C., Berry, A. J., & Jackson, I. (2018). Redox-influenced seismic properties of upper-mantle olivine. *Nature*, *555*(7696), 355–358. https://doi.org/10.1038/nature25764

Dai, L., Hu, H., Jiang, J., Sun, W., Li, H., Wang, M., et al. (2020). Electrical conductivity of major minerals in the upper mantle and transition zone. *Materials*, *13*(2), 408. https://doi.org/10.3390/ma13020408

Dai, L., & Karato, S. (2014a). High and highly anisotropic electrical conductivity of the asthenosphere due to hydrogen diffusion in olivine. *Earth and Planetary Science Letters*, *408*, 79–86. https://doi.org/10.1016/j.epsl.2014.10.003

Dai, L., & Karato, S. (2014b). Influence of FeO and H on the electrical conductivity of olivine. *Physics of the Earth and Planetary Interiors*, *237*, 73–79. https://doi.org/10.1016/j.pepi.2014.10.006

Dai, L., & Karato, S. (2014c). Influence of oxygen fugacity on the electrical conductivity of hydrous olivine: Implications for the mechanism of conduction. *Physics of the Earth and Planetary Interiors*, *232*, 57–60. https://doi.org/10.1016/j.pepi.2014.04.003

Dai, L., Li, H., Li, C., Hu, H., & Shan, S. (2010). The electrical conductivity of dry polycrystalline olivine compacts at high temperatures and pressures. *Mineralogical Magazine*, *74*(5), 849–857. https://doi.org/10.1180/minmag.2010.074.5.849

De Hoog, J. C. M., Gall, L., & Cornell, D. H. (2010). Trace-element geochemistry of mantle olivine and application to mantle petrogenesis and geothermobarometry. *Chemical Geology*, *270*(1–4), 196–215. https://doi.org/10.1016/j.chemgeo.2009.11.017

Faul, U. H., Cline, C. J., David, E. C., Berry, A. J., & Jackson, I. (2016). Titanium-hydroxyl defect-controlled rheology of the Earth's upper mantle. *Earth and Planetary Science Letters*, *452*, 227–237. https://doi.org/10.1016/j.epsl.2016.07.016

Faul, U. H., & Jackson, I. (2007). Diffusion creep of dry, melt-free olivine. *Journal of Geophysical Research*, *112*, B04204. https://doi.org/10.1029/2006JB004586

Karato, S. (1974). *Lattice defects and transport properties of olivine* (p. 56). Tokyo: Geophysics. University of Tokyo.

Karato, S. (1989). Grain growth kinetics in olivine aggregates. *Tectonophysics*, *155*, 255–273.

Karato, S. (1990). The role of hydrogen in the electrical conductivity of the upper mantle. *Nature*, *347*(6290), 272–273. https://doi.org/10.1038/347272a0

Karato, S. (2008). *Deformation of Earth materials: Introduction to the rheology of the solid Earth*. Cambridge: Cambridge University Press. https://doi.org/10.1017/CBO9780511804892

Karato, S. (2012). On the origin of the asthenosphere. *Earth and Planetary Science Letters*, *321/322*, 95–103.

Karato, S. (2015). Some notes on hydrogen-related point defects and their role in the isotope exchange and electrical conductivity in olivine. *Physics of the Earth and Planetary Interiors*, *248*, 94–98. https://doi.org/10.1016/j.pepi.2015.08.007

Karato, S. (2019). Some remarks on hydrogen-assisted electrical conductivity in olivine and other minerals. *Progress in Earth and Planetary Science*, *6*(1), 55. https://doi.org/10.1186/s40645-019-0301-2

Karato, S., & Jung, H. (2003). Effects of pressure on high-temperature dislocation creep in olivine polycrystals. *Philosophical Magazine A*, *83*(3), 401–414. https://doi.org/10.1080/0141861021000025829

Karato, S., Paterson, M. S., & Fitz Gerald, J. D. (1986). Rheology of synthetic olivine aggregates: Influence of grain-size and water. *Journal of Geophysical Research*, *91*(B8), 8151–8176. https://doi.org/10.1029/JB091iB08p08151

Karato, S., & Wang, D. (2013). Electrical conductivity of minerals and rocks. In S. Karato (Ed.), *Physics and chemistry of the deep Earth* (pp. 145–182). New York: Wiley-Blackwell. https://doi.org/10.1002/9781118529492.ch5

Kittel, C. (1986). *Introduction to solid state physics* (6th ed.). New York: John Wiley & Sons.

Kohlstedt, D. L., Keppler, H., & Rubie, D. C. (1996). Solubility of water in the α, β and γ phases of $(Mg,Fe)_2SiO_4$. *Contributions to Mineralogy and Petrology*, *123*(4), 345–357. https://doi.org/10.1007/s004100050161

McCarthy, C., Takei, Y., & Hiraga, T. (2011). Experimental study of attenuation and dispersion over a broad frequency range: 2. The universal scaling of polycrystalline materials. *Journal of Geophysical Research*, *116*, B09204. https://doi.org/10.1029/2011JB008382

Mei, S., & Kohlstedt, D. L. (2000a). Influence of water on plastic deformation of olivine aggregates, 1. Diffusion creep regime. *Journal of Geophysical Research*, *105*(B9), 21,457–21,469. https://doi.org/10.1029/2000JB900179

Mei, S., & Kohlstedt, D. L. (2000b). Influence of water on plastic deformation of olivine aggregates, 2. Dislocation creep regime. *Journal of Geophysical Research*, *105*(B9), 21,471–21,481. https://doi.org/10.1029/2000JB900180

Morishima, H., Kato, T., Suto, M., Ohtani, E., Urakawa, S., Utsumi, W., et al. (1994). The phase boundary between α- and β-Mg_2SiO_4 determined by in situ X-ray observation. *Science*, *265*(5176), 1202–1203. https://doi.org/10.1126/science.265.5176.1202

Paterson, M. S. (1982). The determination of hydroxyl by infrared absorption in quartz, silicate glass and similar materials. *Bulletin de Mineralogie*, *105*(1), 20–29. https://doi.org/10.3406/bulmi.1982.7582

Phillips, J. C. (1973). *Bonds and bands in semiconductors*. New York: Academic Press.

Roberts, J. J., & Tyburczy, J. A. (1993). Impedance spectroscopy of single and polycrystalline olivine: Evidence for grain boundary transport. *Physics and Chemistry of Minerals*, *20*, 19–26.

Schock, R. N., Duba, A. G., & Shankland, T. J. (1989). Electrical conduction in olivine. *Journal of Geophysical Research*, *94*(B5), 5829–5839. https://doi.org/10.1029/JB094iB05p05829

Tollan, P., Smith, R. B., O'Neill, H. S. C., & Hermann, J. (2017). The responses of four main substitution mechanisms of H in olivine to H_2O activity at 1050°C and 3 GPa. *Progress in Earth and Planetary Science*, *4*(1), 14. https://doi.org/10.1186/s40645-017-0128-7

Tollan, P. M. E., O'Neil, H. S. C., & Hermann, J. (2018). The role of trace elements in controlling H incorporation in San Carlos olivine. *Contributions to Mineralogy and Petrology*, *173*(11), 89. https://doi.org/10.1007/s00410-018-1517-7

Wang, D., Mookherjee, M., Xu, Y., & Karato, S. (2006). The effect of water on the electrical conductivity in olivine. *Nature*, *443*(7114), 977–980. https://doi.org/10.1038/nature05256

Xu, Y., Shankland, T. J., & Duba, A. G. (2000). Pressure effect on electrical conductivity of mantle olivine. *Physics of the Earth and Planetary Interiors*, *118*(1–2), 149–161. https://doi.org/10.1016/S0031-9201(99)00135-1

Yoshino, T., & Katsura, T. (2013). Electrical conductivity of mantle minerals: Role of water in conductivity anomalies. *Annual Review of Earth and Planetary Sciences*, *41*(1), 605–628. https://doi.org/10.1146/annurev-earth-050212-124022

Zhang, J., Li, B., Utsumi, W., & Liebermann, R. C. (1996). In situ X-ray observations of the coesite–stichovite transition: Reversed phase boundary and kinetics. *Physics and Chemistry of Minerals*, *23*, 1–10.